Quaternary Science Reviews 247 (2020) 106574

Contents lists available at ScienceDirect

Quaternary Science Reviews

journal homepage: www.elsevier.com/locate/quascirev

Reconstructing East African monsoon variability from grain-size distributions: End-member modeling and source attribution of diatom-rich sediments from Lake Chala

Inka Meyer [a, *], Maarten Van Daele [a], Niels Tanghe [a], Marc De Batist [a], Dirk Verschuren [b]

[a] Renard Centre of Marine Geology (RCMG), Department of Geology, Ghent University, Krijgslaan 281 S8, B-9000, Gent, Belgium
[b] Limnology Unit, Department of Biology, Ghent University, Ledeganckstraat 35, B-9000, Gent, Belgium

ARTICLE INFO

Article history:
Received 29 May 2020
Received in revised form
25 August 2020
Accepted 30 August 2020
Available online xxx

Keywords:
Equatorial Africa
Holocene
Paleolimnology
Clastic sediment
Sediment provenance
Paleoclimatology

ABSTRACT

Grain-size analysis and end-member modeling of the clastic fraction of the 25-kyr sediment sequence from Lake Chala, a meromictic crater lake on the lower east slope of Mt. Kilimanjaro, reveal crucial aspects of climate-driven environmental change in equatorial East Africa since the Last Glacial Maximum. The finely laminated sediments of Lake Chala contain only up to 40% of clastic components, the rest are mainly diatom frustules and amorphous organic matter. Measured grain-size distributions were split into six statistically meaningful end members, of which four could be linked to a distinct source and transport mechanism of clastic mineral input: fine aeolian dust from distal sources (EM1), fine catchment runoff (EM2), coarser aeolian dust from proximal sources (EM5) and coarse erosive material from the upper crater slopes (EM6). The two other end members (EM3 and EM4) represented frustules of the two most common diatom taxa in Lake Chala, *Afrocymbella barkeri* and *Nitzschia fabiennejansseniana*, which had (partly) survived sample pre-treatment.

Temporal variation in normalized abundance of the two dust-derived end members are valuable proxies for past changes in monsoon circulation over equatorial East Africa. During Northern Hemisphere cold periods (e.g., Last Glacial Maximum and Younger Dryas) the Inter-Tropical Convergence Zone shifted southward, enhancing northeasterly monsoon winds in the Lake Chala area and increasing advection of fine dust from the dry Horn of Africa region. Simultaneously, more modest continental heating reduced the prevalence of small-scale atmospheric turbulence, and thus the occurrence of dust devils, resulting in reduced influx of coarse dust from drylands nearby. Conversely, abrupt intensification of the south-easterly monsoon at the onset of the Holocene is recorded by an abrupt increase in the amount of coarse dust delivered to Lake Chala. Temporal variation in the end members representing catchment run-off (EM2) and erosion (EM6) mainly reflect changes in lacustrine sedimentation dynamics associated with major lake-level fluctuation, as evidenced by other paleoenvironmental proxies. Overall this study shows that subdivision of the clastic fraction of lacustrine sediments into statistically robust grain-size end members can provide multiple independent and quantitative proxies which help constrain reconstructions of a region's multi-faceted climate history.

1. Introduction

Terrigenous mineral particles deposited in all kinds of sedimentary records (terrestrial, marine and lacustrine) contain valuable information for paleoclimate and paleoenvironmental reconstruction (Stuut et al., 2002; Meyer et al., 2013; Liu et al., 2016; Ben-Israel et al., 2017). By definition, terrigenous sediments derive from on-land sources and are transported to the site of deposition by different mechanisms driven by moving ice, water or wind. Their occurrence and abundance is influenced by the geological setting, availability of unconsolidated deposits in the source area and the energy required for initial lift-up and transport (Tsoar and Pye, 1987). On a global scale, fluvial (including overland) flow is the most important transport mechanism (Milliman and Syvitski, 1992). However, particle transport by wind (aeolian transport) can be important as well, especially in regions with (semi-) arid

* Corresponding author.
E-mail address: inka.meyer@ugent.be (I. Meyer).

https://doi.org/10.1016/j.quascirev.2020.106574

climate regimes. Consequently, terrigenous deposits typically represent a mixture of sediments with different provenances and supplied to the site by different processes (Weltje and von Eynatten, 2004; Weltje and Prins, 2007). This results in characteristic bi- or even polymodal grain-size distributions, which are challenging to interpret in terms of past climate or environmental conditions (Meyer et al., 2013). To overcome this problem, so-called end-member models have been developed (Weltje, 1997; Weltje and Prins, 2007; Dietze et al., 2014; Paterson and Heslop, 2015). These mathematical-statistical models explain the grain-size variation as resulting from a combination or mixing of statistically robust sub-populations of particles, the grain-size end members. Each end member is assumed to represent a fraction of particles that has the same provenance and/or was transported by the same process to the site of deposition. By mathematically unmixing this polymodal signal, the individual end members can be isolated.

This 'unmixing' of the clastic sediment fraction has already been successfully applied in paleoenvironmental reconstructions on Quaternary time scales in many regions, such as Western Australia (Stuut et al., 2014), the North Atlantic (Prins et al., 2002), the Tibetan Plateau (Liu et al., 2016), and offshore West Africa (Stuut et al., 2002; Tjallingii et al., 2008; Just et al., 2012; Meyer et al., 2013). Contrary to long-term climate dynamics in West Africa, which are dominantly tied to variability in the tropical Atlantic (so-called 'African') monsoon, climate dynamics in East Africa are tied to three different monsoon systems, namely the southeasterly and northeasterly Indian Ocean monsoons as well as the tropical Atlantic-based monsoon system. Consequently many more records are required to fully document the spatiotemporal patterns of past climate change across the East African sub-continent. Especially sediment records from close to the Equator in East Africa may hold important information on low-latitude climate processes, and their interaction with high-latitude climate dynamics (Verschuren et al., 2009).

This study investigates the terrigenous (clastic) fraction of lacustrine sediments in Lake Chala, a deep crater lake near Mt. Kilimanjaro in equatorial East Africa. Extensive studies have already been performed on Lake Chala itself and its sedimentary infill, mainly in the framework of the European Science Foundation (EFS)'s EuroCLIMATE project CHALLACEA (2005–2008). Reconstruction of past lake-level fluctuations using seismic stratigraphy (Moernaut et al., 2010) and sediment lithology (Wolff et al., 2011) revealed that Lake Chala has experienced several lowstand episodes during the last 25,000 years (25 ka) but maintained a stratified water column throughout, hence providing one of the few continuous lake records from East Africa covering both the Last Glacial Maximum (LGM) and complete post-glacial period (Verschuren et al., 2009). However, the clastic fraction of Lake Chala sediments thus far remained unstudied, in part because of the sediments' high diatom and organic-matter content (Barker et al., 2011, 2013), and hence rather low abundance of detrital components. Nevertheless, understanding the processes that control transport and deposition of clastic sediment particles to the lake may provide important information about the history of climate-driven hydrological change or of past variations in wind direction and strength. Therefore, we conducted a detailed investigation of the clastic sediment fraction of Lake Chala based on grain-size analysis, including end-member modeling in order to define robust sub-populations of the mineral particles. Special attention is given to methodological complications arising from the abundant presence of diatoms. The findings of this study close a gap in understanding the Lake Chala sedimentary archive, thereby creating a depositional framework for paleoenvironmental reconstruction in a region extremely sensitive to changes in monsoon dynamics.

2. Study area

2.1. Geological and limnological setting

Lake Chala (3°19′S, 37°42′E), located on the border between Tanzania and Kenya, is a freshwater lake filling a volcanic caldera at an altitude of 880 m above sea level (a.s.l.) on the lower east slope of Mt. Kilimanjaro (Fig. 1a). The lake has a surface area of 4.2 km^2, and its maximum water depth has fluctuated between 92 and 98 m in the last two decades (Moernaut et al., 2010; D. Verschuren et al. personal observation). The lake is entirely surrounded by rocky and steep crater walls, reaching a height of up to 170 m above the lake surface and limiting its catchment area to only 1.38 km^2 (Fig. 1b) (Buckles et al., 2014). Annual evaporation from the lake surface far exceeds local rainfall, therefore the water balance of Lake Chala is controlled by subsurface in- and outflow (Verschuren et al., 2009). Subsurface inflow originates from percolation of precipitation higher up on Mt. Kilimanjaro, primarily in the upper montane forest and adjacent subalpine zone (Hemp, 2005; Bodé et al., 2020), reaching the lake 3–4 months later (Barker et al., 2011). A small ravine of ~300 m long breaches the NW corner of the crater rim (Fig. 1b), with a creek that is most often dry but occasionally activated during episodes of intense local rainfall (Buckles et al., 2014). Dry-season water-column mixing extending to between 45 and 60 m water depth (Wolff et al., 2014) regenerates nutrients to the photic zone to support high diatom productivity from July until September (Wolff et al., 2011). The lower water column of Lake Chala is permanently stratified and anoxic, classifying the lake as meromictic.

High-resolution (3.5 kHz) bottom-profiling and reflection seismic profiles, obtained in 2003, revealed a characteristic bowl-shaped bathymetry of the crater basin filled with ~210 m of lacustrine sediments (Fig. 1b) (Moernaut et al., 2010). The steep inner crater walls continue below the water surface, with peripheral bottom slopes dipping between 30° and 90°, decreasing to more gently dipping slopes (1–5°) below depths of 60–70 m. A depositional sequence of alternating basin-focused and draped sedimentary units allowed Moernaut et al. (2010) to reconstruct a detailed history of past lake-level fluctuations over the past ~140 ka. The last 25 ka of this lake-level history is consistent with a century-scale reconstruction of past variation in local precipitation based on the Branched and Isoprenoid Tetraether (BIT) index of sedimentary bacterial lipids (Verschuren et al., 2009).

2.2. Present-day climatic setting

The climate of equatorial East Africa is mainly controlled by the seasonal passage of rain belts associated with the Inter-Tropical Convergence Zone (ITCZ) and the Congo Air Boundary (CAB; Fig. 2a and c). The CAB is the convergence zone between winds and moisture originating from the Atlantic and Indian Oceans, thus creating a west-to-east zonal gradient in hydroclimate across the East African plateau. Due to its location far east of the CAB (Fig. 2a), the influence of Atlantic Ocean moisture is minimal at Lake Chala, both now and likely throughout the late Quaternary (Verschuren et al., 2009). Situated at the foot of Mt. Kilimanjaro, the local climate at Lake Chala is classified as tropical semi-arid. As peak insolation crosses the equator twice yearly during the equinoxes, rainfall occurs predominantly from March to May ('long rains') and from October to December ('short rains') (Fig. 2b and c) (Nicholson, 2000). The long rains are associated with the southeasterly monsoon, and typically represent the major portion of annual precipitation; the short rains are associated with the northeasterly monsoon, and display stronger inter-annual variability because they are more sensitive to changes in Indian Ocean sea-surface

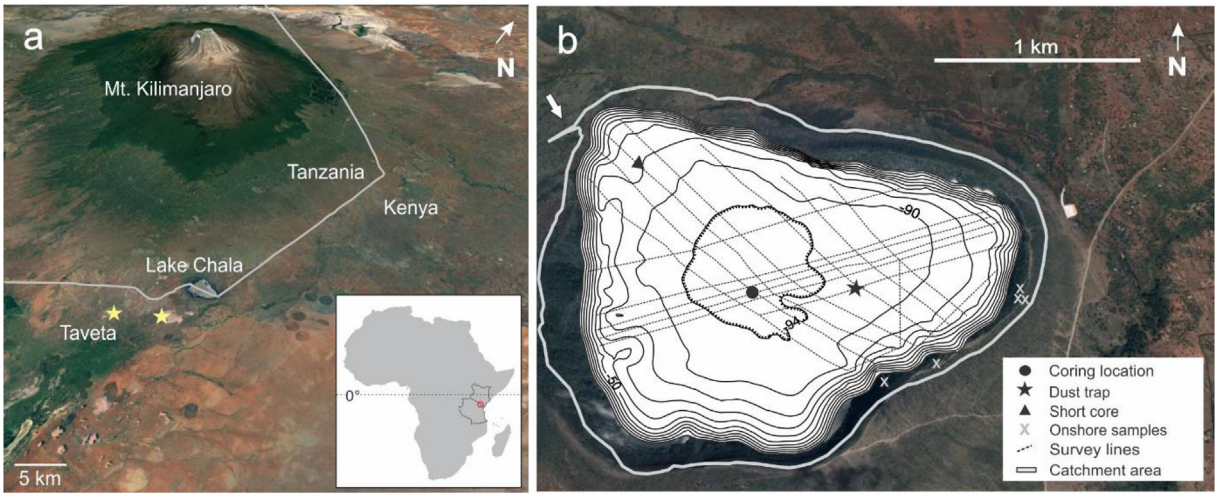

Fig. 1. Setting of Lake Chala. a) Google Earth image of the Mt. Kilimanjaro area in eastern equatorial Africa, with Lake Chala (red dot in inset map) situated on its lower eastern flank and bridging the border between Kenya and Tanzania. Yellow stars show the locations of two dust traps. b) Bathymetry of Lake Chala inside its crater-basin catchment area (grey line), showing that steep inner crater walls continue under water in peripheral lake areas. Depth contours until 90 m are drawn at 10-m intervals; the maximum depth of 94 m (in 2003) is indicated by the innermost contour line. Also indicated are the locations of the ephemeral creek breaching the NW corner of the crater rim (white arrow), the 25-ka CHALLACEA core site (black dot), a short surface core also analyzed in this study (black triangle), a temporary dust trap on the lake (black star) and onshore soil samples (white crosses). Modified from Moernaut et al. (2010). (For interpretation of the references to color in this figure legend, the reader is referred to the Web version of this article.)

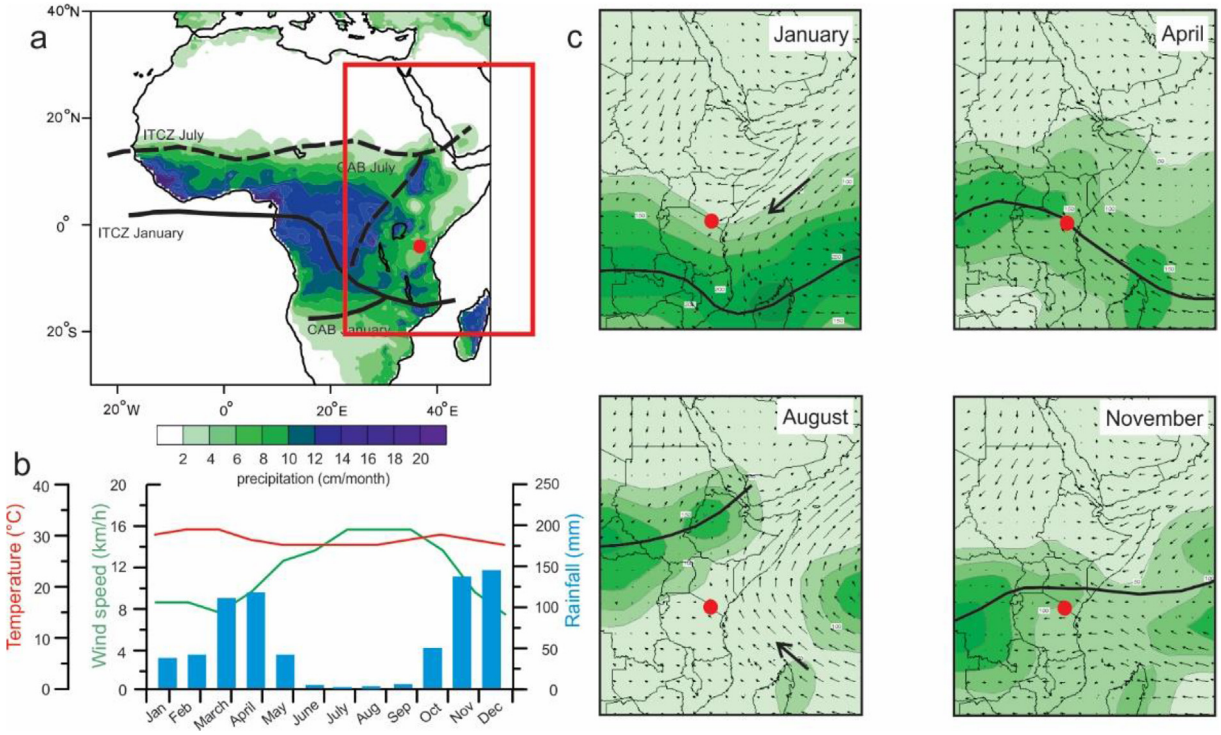

Fig. 2. Climatic setting at Lake Chala. a) Seasonal migration of the Inter-Tropical Convergence Zone (ITCZ) and Congo Air Boundary (CAB), and associated rain belt between July (dashed line) and January (full line) superimposed on the distribution of total annual rainfall across the African continent (green to blue tones, expressed as mean monthly precipitation in cm; obtained from the University of Delaware database; http://climate.geog.udel.edu/_climate/). The red dot is the location of Lake Chala and the red box delineates the area of eastern Africa covered by the season-specific maps in panel c. b) Maximum monthly temperature, wind speed and rainfall for the town of Voi, ~100 km east of Lake Chala (http://weatherwx.com). c) Synoptic climatology of eastern Africa for four representative months in each season, in relation to Lake Chala (red dot). Green shading shows monthly precipitation at 50-mm intervals, in relation to the ITCZ position (thick black line) and vectors (arrow direction and length) of wind at 925 hPa (http://iridl.ldeo.columbia.edu). Thick arrows indicate the dominant wind direction in January and August, respectively. (For interpretation of the references to color in this figure legend, the reader is referred to the Web version of this article.)

temperature (Black et al., 2003; Tierney et al., 2013). Mean annual precipitation at the town of Taveta, 7 km south of Lake Chala, is 583 mm (Hemp, 2006) with major interannual variation, as is typical for semi-arid tropical regions. Most of the low-elevation landscape around Chala crater is covered with dry grass and scrub savannah (Griepentrog et al., 2019), with non-vegetated (exposed) soils common in floodplains and around human settlements.

The exceptionally large latitudinal range of seasonal ITCZ migration in East Africa (15° N to 15° S; Fig. 2a) enhances the region's monsoonal wind dynamics. East African monsoons are relatively dry, because northeasterly monsoonal winds pass over the Arabian Peninsula and cool waters in the Arabian Sea, while southeasterly monsoonal winds lose most of their humidity along the East African coast due to friction with the coastline (Nicholson, 1996). Wind speeds at Lake Chala are variable but generally low under north-east monsoonal influence from November to April and stronger under south-east monsoonal influence from May to October when the ITCZ is displaced northward (Wolff et al., 2014). Given incomplete vegetation cover in the Chala area, sediment transport by wind is common. This can take the form of dust devils, a small-scale phenomenon generated by intense local surface heating (Fig. 3a), or as a wall of dust raised by severe turbulence within thunderstorms moving over the area (Fig. 3b).

3. Material and methods

3.1. Core sampling and preparation

In 2005, a 21.65 m-long composite sediment core was retrieved from the center of Lake Chala, covering the past 25 ka (Verschuren et al., 2009). This lake record consists almost entirely of finely laminated sediments, including long sections of varves each comprising a dark-light lamination couplet. The dark laminae mainly consist of amorphous organic matter and fine-grained mineral particles, supplemented by calcite crystals only in the upper half of the sequence (Wolff et al., 2011). The typically thicker light laminae are mainly composed of diatom frustules, predominantly *Afrocymbella barkeri* (Cocquyt and Ryken, 2016) and several *Nitzschia* spp. which together account for over 90% of the diatom assemblage (Barker et al., 2013). The chronology of this record was established through ^{210}Pb and high-resolution AMS ^{14}C dating, producing an age model which confirmed the varved character of the sediments (Blaauw et al., 2011) although only few sections can be easily counted (Wolff et al., 2011). The sequence also contains five turbidites (48, 42, 5, 6 and 14 cm thick) and three mm-scale tephra layers, the boundaries of which stand out from the finely laminated matrix sediment. These event deposits were not sampled for this study.

Samples for grain-size analysis were taken as 4-cm core increments at depth intervals of 12 cm throughout the composite sediment sequence (excluding the event deposits), with a few extra samples in the core section encompassing the Younger Dryas (YD) chronozone (12.9–11.6 ka BP) resulting in a local sampling resolution of 4 or 8 cm. This yielded a total of 172 samples each representing ~40 years of deposition at ~150-year intervals on average. In the following, sample depth refers to the center depth of each sampled core increment. Prior to grain-size analysis, sample solutions were treated by boiling with H_2O_2 (35%) and HCl (10%) to remove organic matter and carbonates, respectively. Detailed laboratory tests revealed that the abundant biogenic silica (diatoms) could not be removed with standard procedures, which is a treatment with 2*N* NaOH (Meyer et al., 2013), without destroying or damaging the fragile, clay-sized mineral particles. Therefore diatoms were removed, as much as possible, by flotation in sodium polytungstate ($Na_6(H_2W_{12}O_{40})H_2O$), a non-toxic heavy liquid (density of 2.8 g/ml), described to be a reliable method to separate diatoms from clastic sediment components without biasing them (Shemesh et al., 1995). To separate the lighter diatom fraction from the heavier detrital mineral fraction, here the heavy liquid was diluted with distilled water to a density of 2.1 g/ml. Prior to heavy liquid separation, the clay fraction (<4 μm) was removed by gravitational settling (Atterberg method) using Stokes' Law (Müller, 1967). Afterwards this clay-sized mineral fraction was again combined with the heavier sediment components (now mostly consisting of the larger mineral particles, but still also a significant amount of diatoms; cf. below). Finally, immediately before grain-size measurement the samples were boiled in 2% sodium hexametaphosphate to ensure complete disaggregation of the particles.

3.2. Dust-trap samples and onshore reference soils

During fieldwork for the International Continental Scientific Drilling Program (ICDP) project DeepCHALLA in November 2016, three dust traps were installed to monitor the *in-situ* dust input to Lake Chala. One dust trap was installed on the offshore drilling platform and was operated during three weeks of the drilling (Fig. 1b). The other two dust traps were installed on roof tops within ~7 km of the lake permanently and are partly analyzed in this study. In addition, five soil samples from different locations on the southeastern crater rim (Fig. 1b) were also available for grain-size analysis. Prior to measurement both the dust and soil

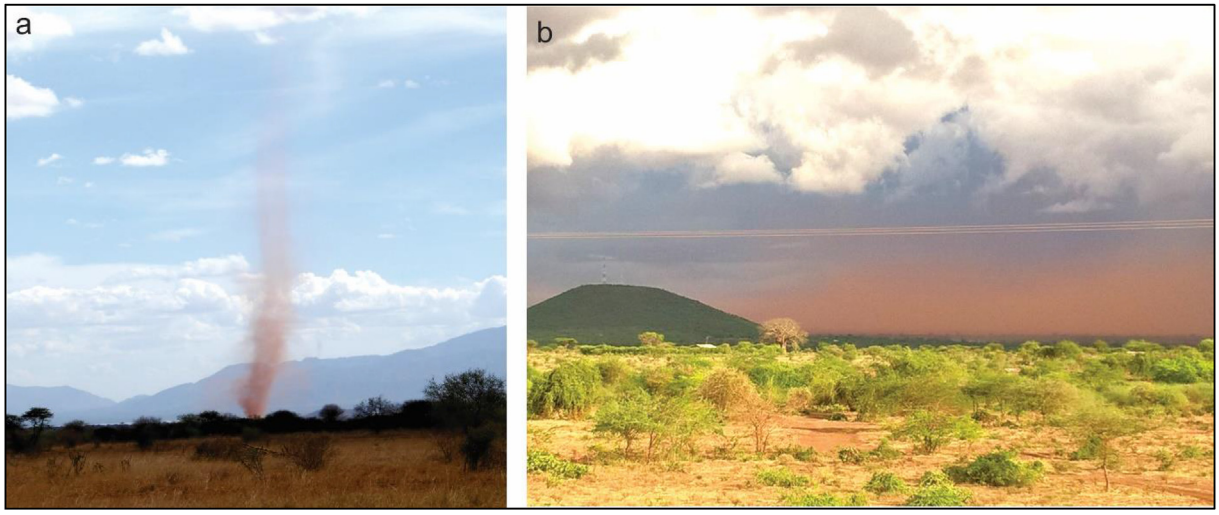

Fig. 3. Dust transport in the Lake Chala area. a) Inside dust devils racing across the landscape, dust is lifted up high into the air and transported over considerable distances (photo by Inka Meyer, November 2016). b) Wall of dust raised by the turbulence beneath an approaching thunderstorm (photo by Dirk Verschuren, November 2016).

samples were chemically treated to remove the organic matter and carbonates and to disaggregate, as described above.

3.3. Grain-size measurement and end-member modeling

Grain-size distributions (GSDs) of the pre-treated sediment, dust-trap and surface soil samples were obtained by laser diffraction, using a Malvern Mastersizer 3000 instrument. The samples were inserted via a Hydro MV module, and sample quantity was adjusted to obtain a laser-beam obscuration between 10% and 20%. An average GSD for each sample (n = 172), determined by three repeat measurements, was used as input data for end-member analysis. Unmixing of the obtained GSD was performed using the AnalySize modeling algorithm (Paterson and Heslop, 2015), which is inspired by the unmixing done in hyperspectral image analysis and available as a free, MATLAB-based GUI software package (https://github.com/greigpaterson/AnalySize). The method aims to establish a physical mixing model that transforms the measured GSDs in a limited number of non-negative and unimodal grain-size end members (EMs) that can be interpreted individually. The minimum number of EMs required for a satisfactory approximation of the data is estimated by calculating the coefficient of determination (r^2), representing the proportion of the variance of each grain-size class that can be reproduced by the approximated data. Further technical aspects of AnalySize are described in detail by Paterson and Heslop (2015).

3.4. Estimating the theoretical range of diatom particle-size distributions

Despite the multi-step sample-treatment procedure to remove the abundant diatoms in Lake Chala sediments, examination of the samples by microscope prior to grain-size analysis showed a variable and often significant amount of diatoms still remaining. To account for this contamination in grain-size distributions, we developed a method to discriminate and extract the potential grain-size EMs produced by those diatoms. For this purpose we estimated theoretical ranges for the particle-size distributions of *Afrocymbella barkeri* and *Nitzschia fabiennejansseniana*, the two most common diatom taxa in the CHALLACEA record (Barker et al., 2013), as would be recorded by the Malvern Mastersizer laser beam. First we approximated the shape of the diatom frustules as a short straight rhombic prism (*A. barkeri)* and a (tall) square cuboid (*N. fabiennejansseniana*) (Fig. 4), using the minimum and maximum frustule dimensions for these species reported by Cocquyt and Ryken (2016, 2017): 19.9–63.8 μm long by 8.2–13.7 μm wide (*A. barkeri*) and 24.0–48.5 μm long by 2.1–2.8 μm wide (*N. fabiennejansseniana*). Using a MATLAB script (see Supplementary Information) we created 301 congruent diatom frustules of each type, with dimensions normally distributed between the prescribed minimum and maximum sizes, using these ranges as the 99.7% confidence interval (i.e. mean ± three standard deviations). Then, to mimic the different angles at which a diatom frustule can pass the laser beam, we determined for each of these shapes the length of all line segments through the center of gravity at angular distances of 1°, resulting in 20,260 line-segment lengths per shape (or >6.2 million for all 301 shapes of each type) (Fig. 4). Because laser-diffraction GSDs are plotted as volume percentages under the assumption that all particles are spheres, we treated each line-segment length as the diameter of a sphere to calculate a volume. Finally, we divided the resulting dataset in 100 log-equal bins between 1 and 100 μm to derive theoretical diatom GSDs. These GSDs are evidently only an approximation, as no Mie solution (theory used by the Malvern software; https://www.malvernpanalytical.com) for scattering of such geometries exists. Furthermore, the diatom frustules will scatter laser light not only along their center but in all areas of their elongated form. As the chance for scattering is greater along the long axes of the modeled shapes, the resulting GSDs may underestimate shorter lengths. Nevertheless, we believe that our theoretical diatom GSDs provide a good first-order approximation of the range of grain sizes to be expected for each diatom type.

3.5. Relating grain-size distribution to bulk-sediment composition

The relative abundance of each particle population in the GSDs is expressed as the percent (%) abundance of the modeled EMs summed to 100%. To optimize interpretation of down-core variation in the relative abundance of each EM in terms of changes in particle flux and sedimentation dynamics through time, we also calculated the percent abundance of the non-diatom EMs relative to bulk dry-mass sediment composition. For this purpose, the percent abundance of clastic sediment components was calculated as the dry mass left after subtracting the percent abundances of organic matter (OM), authigenic carbonates (here mostly calcite; Wolff et al., 2011) and biogenic silica (bSi). OM content was calculated from organic-carbon (OC) values (Barker et al., 2013) using a regression of OM versus OC (r^2 = 0.603) based on 111 paired measurements of OC and OM in the uppermost 2.52 m of the sequence; the latter was determined with the loss-on-ignition method (Dean, 1974). Carbonate ($CaCO_3$) content was calculated from inorganic-carbon (IC) values determined at the GeoForschungsZentrum Potsdam as the difference between OC content and total carbon content, using a DELTAplusXL mass spectrometer equipped with a Carlo Erba elemental analyser. BSi content data (Barker et al., 2013) were obtained by digesting sediment samples in 1% Na_2CO_3 for 3 h at 85 °C in a heated shaking bath, and spectrophotometrically measuring the dissolved silica (Conley and Schelske, 2001).

4. Results

The mineral fraction of profundal Lake Chala sediments has a fine-grained, silty to clayey texture with a dominant mode around 10 μm (Fig. 5a). However, overlay of all samples (n = 172) clearly reveals a polymodal grain-size distribution, hence, the GSD data set requires end-member analysis. Goodness-of-fit statistics show an increasingly better fit (higher r^2) with the raw GSD spectra as the number of EMs is increased (Fig. 5b). However, for meaningful interpretation of the observed compositional variation a relatively modest number of such populations is advocated (Weltje and Prins, 2007). Here we chose a model with six EMs, together explaining 99.6% of the observed GSDs, to best represent the entire data set. The modeled mean modal sizes of these EMs are 2.1 μm (EM1), 4.0 μm (EM2), 10.0 μm (EM3), 19.8 μm (EM4), 60.6 μm (EM5) and 329.6 μm (EM6) (Fig. 5c). A modest peak centered on 0.6 μm (size range 0.3–1 μm) observed in most GSDs (Fig. 5a) was not represented in any of the end-member model runs (Fig. 5c), and can be attributed to noise due to Rayleigh scattering by off particles >1 μm.

The relative abundance of EM1 varies between ~1% and ~9% of the measured GSDs (Fig. 6), with highest values occurring in the lower half of the record. In the upper 8 m the EM1 values are mostly below 3%, but they increase again in the uppermost 1.5 m to ~5% near the surface. EM2 covers a much wider range of values, between complete absence (i.e., 0%) and ~65%. Between 17 and 11 m depth its abundance is rather high (typically >30%), followed by a decreasing trend culminating in a distinct minimum between 8.8 m and 8.2 m. From 8 to 2 m values are high again (>30%), followed by fluctuating but overall decreasing values in the uppermost part of the sequence. EM3 is the overall most abundant particle fraction in

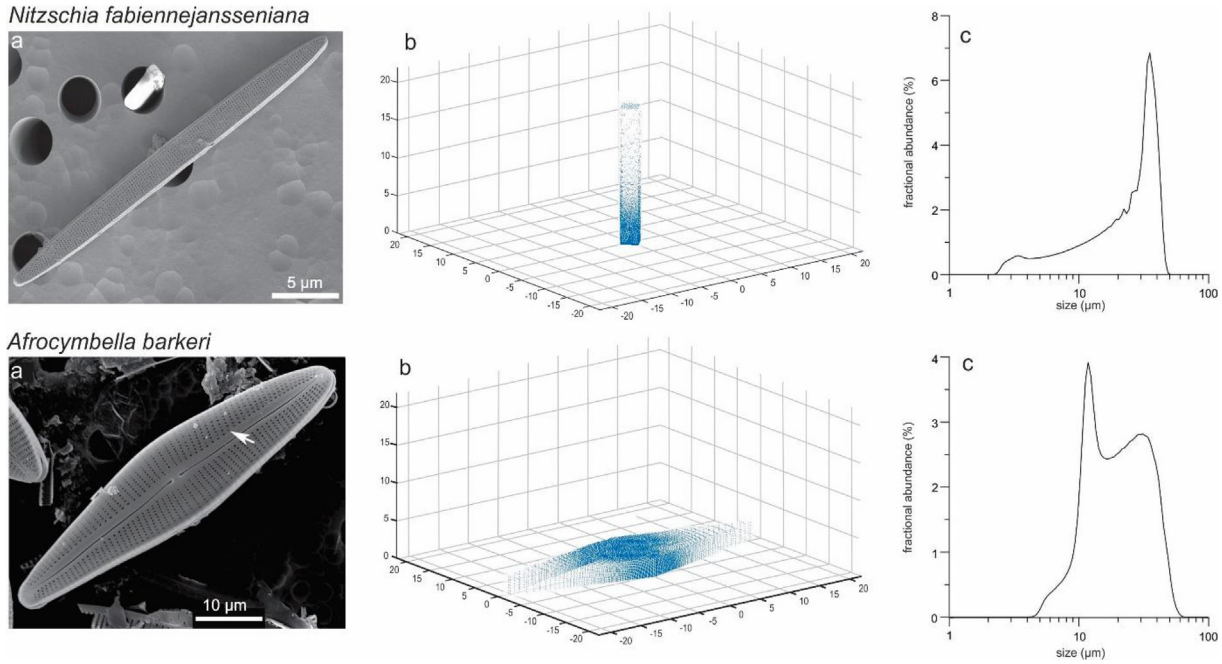

Fig. 4. Diatom productivity in Lake Chala is dominated by two species, the needle-shaped *Nitzschia fabiennejansseniana* (upper panels) and rhomboid *Afrocymbella barkeri* (lower panels). a) SEM images of both species in top view, with scale (courtesy of Christine Cocquyt, Botanic Garden Meise); b) intersections of 20,260 line segments with the outer boundary of simplified shapes of both diatoms in a three-dimensional coordinate system; c) theoretical grain-size distribution of each diatom species on a logarithmic scale.

the record, but also highly variable with values ranging between ~13% and ~80%. Generally the trends in its abundance are opposite to those of EM2. High EM3 abundances (30–80%) are recorded in the deepest part of the record (below 18 m), and lowest values (<20%) between 15.5 and 13 m depth. This is followed by an increasing trend, reaching a peak value of 72% around 8.7 m. Above this level EM3 values are again lower (stabilizing around 30%), until they start increasing again from 2.4 m depth to reach values averaging 50% near the surface.

EM4 varies between 0% and 39.7%. In the lower half of the record (below 11.5 m depth) its abundance averages 9.4%, whereas in the upper half its average is 18.5% with increasing values towards the top. Also the abundance of EM5 can be divided in two parts, with lower values (on average 2.6%) below 8 m and higher values (average higher than 6%) above that level. The abundance of EM6 fluctuates, but is generally low (on average 3.7%, with 11.2% as highest value), and lacking a clear trend except that its lowest abundances occur in the uppermost 2.5 m.

5. Discussion

5.1. Association of grain-size end members with diatoms

In the end-member approach all six particle populations are modeled to have a unimodal grain-size distribution (Fig. 5c). However, any particle population representing the diatoms that survived sample pre-treatment can be expected to have a polymodal and poorly sorted grain-size distribution, depending on the diatoms' orientation in the laser beam. Our theoretical GSDs for the two dominant diatom species in Lake Chala indeed suggest that they should be represented by polymodal distributions, but both with a fairly pronounced dominant mode centered around 10–15 µm and 20–40 µm, respectively (Fig. 4), i.e. close to the mean modal size of EM3 and EM4 (Fig. 5c). Suspecting that these two EMs may indeed represent diatoms, we directly compared the down-core distribution of EM3 and EM4 (as % of total GSD) against the absolute abundance of these two diatom species in untreated sediment (Milne, 2007), and found convincing similarities between the two data sets (Fig. 7). More precisely, %EM3 correlates with the abundance of *Afrocymbella barkeri* ($r^2 = 0.448$, $p < 0.0001$, $n = 168$), and %EM4 with the abundance of *Nitzschia fabiennejansseniana* ($r^2 = 0.202$, $p < 0.0001$; $n = 168$). The lower correlation found for EM4 is consistent with the fact that the fossil diatom assemblages of Lake Chala also include other *Nitzschia* species (Milne, 2007). Moreover, due to their fine and elongated shape a greater portion of them are removed either by dissolution in NaOH or by the heavy liquid separation. We are therefore confident that EM3 and EM4 represent the two dominant diatom species, and exclude them from further discussion of the clastic fraction. Taking into account the relationship between summed EM distributions and the measured ('true') GSD, we are aware that deleting two EMs from the data set potentially results in removal of part of the clastic-mineral GSD. However, given the confirmed association of EM3 and EM4 with the down-core distribution of fossil diatoms, we surmise that excluding them from the GSDs better reveals the down-core distribution of the EMs that do represent mineral particle populations. Thus, we normalized the % abundances of EM1, EM2, EM5 and EM6 against the sum of those four end members, making these values independent of dilution by EM3 and EM4. In the following these normalized EMs are indicated by the prefix 'n'.

5.2. Attribution of clastic particle populations

5.2.1. EM1: distal dust

EM1 represents the finest particle fraction in Lake Chala sediments, with a mean modal grain size of ~2.1 µm (95% range: 0.8–3.0 µm; Fig. 5c). Considering this very small size, we suggest that it reflects fine aeolian dust advected from distal sources. Typically also fine and very fine silt up to 15 µm is classified as fine aeolian dust, which once in suspension can travel over long distances before settling (Pye, 1987; Stuut et al., 2009). Our interpretation is based on the occurrence of a shoulder between 2 and 3 µm

in the combined GSD of three dust-trap samples from the Chala area collected in November 2016 (Fig. 8a). No doubt, the latter samples are a mixture of dust from different sources and, possibly, different wind systems (Fig. 3), but due to their limited number we refrained from subjecting them to a separate end-member analysis.

5.2.2. EM2: fine clastic sediments from soil run-off

With a mean modal size of 4.0 μm (95% range: 1.7–14 μm; Fig. 5c), EM2 represents the fraction of fine silt, which dominates the clastic component of profundal sediments in Lake Chala (Fig. 6). Even a higher proportion of this clay/silt-sized fraction is found at the top of short cores collected in front of the ephemeral creek which breaches the northwestern corner of the Chala crater rim (Figs. 1b and 8b). Therefore we interpret EM2 to represent fine-grained soil run-off, derived not only from the steep inner crater slopes but also from a sizable area of gently sloping land beyond it.

5.2.3. EM5: proximal dust

The mean modal size of EM5 is situated around 60 μm (95% range: 8.8–183 μm; Fig. 5c), identical to the dominant mode of the dust-trap samples from the town of Taveta. Therefore EM5 is interpreted to be transported to the lake by air. However, as its modal grain size is relatively coarse, the source area of this material in the Chala sediment record must be situated in close range from the lake. Coarse aeolian dust is defined to consist of coarse and very coarse silt (grain sizes >15 μm), and to travel closer to the ground than fine dust (Pye, 1987; Stuut et al., 2009; Tsoar and Pye, 1987).

5.2.4. EM6: crater-slope sand

With a mean modal grain size of 330 μm (95% range: 57–1080 μm; Fig. 5c), EM6 represents the coarsest fraction of mineral particles in Lake Chala sediments. Comparison with the GSDs of onshore soil samples show a strong overlap (Fig. 8d). Therefore EM6 is interpreted to be composed of sand-sized erosional material from the inner crater slopes and rim surrounding Lake Chala. Normally, we would expect coarse material to be deposited mostly in nearshore bottom areas. However, in Lake Chala it can also be transported to offshore areas, because much of the inner crater slopes consist of rapidly cooled pyroclastic material containing air bubbles, which makes the particles comparably light and allows them to float or stay in suspension for some time before sinking.

5.3. Paleoenvironmental changes during the last 25 ka inferred from grain-size spectra

In Figs. 9 and 10, the down-core distributions of the four grain-size normalized EMs (nEMs) interpreted to be derived from clastic particle populations are plotted against time. This reveals distinct temporal trends, which can be inferred to reflect paleoenvironmental changes in and around Lake Chala, or further afield, over the past 25,000 years. Temporal trends in nEM2 and nEM6, which we interpret have been transported to the lake by overland run-off, either reflect changes in the prevalence of this transport, or in processes of post-depositional sediment redistribution within the lake. Of these, the fine-grained clastic sediment (nEM2) reaches its highest percent-abundance values during known dry periods in East Africa, such as the late-LGM to early late-glacial period (including the Heinrich-1 chronozone, H1) and the YD (Gasse, 2000; Verschuren et al., 2009; Stager et al., 2011) (Fig. 9). Most pertinently, temporal variation in nEM2 displays an overall inverse correlation with the history of lake-level change in Lake Chala itself, as reconstructed from the sequence of alternating draped (high-stand) and ponded (low-stand) seismic-stratigraphic units (Fig. 9). These include major lake-level declines (on the order of 40–50 m) during the dry climatic conditions which prevailed in the two above-mentioned periods as well as in the mid-Holocene (Verschuren et al., 2009). These episodes of low lake level, and hence more complete water-column mixing, are also testified by reduced preservation of algal pigments in the lake's profundal sediments (Meyer et al., 2018). Moreover, both proxies are consistent with reconstructed variation in local rainfall based on the Branched and Isoprenoid Tetraether (BIT) index of bacterial lipids in Lake Chala sediments, which also shows driest climatic conditions to have occurred during the late-LGM and early late-glacial period, the YD and the mid-Holocene (Verschuren et al., 2009).

Changes in the (relative) abundance of EM2 down-core can potentially result from two different mechanisms. First, the influx of fine-grained clastic sediment to Lake Chala may be enhanced during low-stand periods because of the enlarged catchment. In the steep-sided crater basin of Lake Chala, however, such enhancement would likely be minimal because even a drawdown of 50 m increases the catchment area by less than 10% (Fig. 1b), and all of this extra catchment would consist of rocks rather than erodible soils. Alternatively it might be proposed that the climatic drought that caused the drawdown also created a diminished vegetation cover within the crater, which in turn would have made more soil subject to mobilization during precipitation events. However, vegetation reconstructions from Lake Chala (Damsté et al., 2011; van Geel et al., 2011) indicate that at this time scale the region's plant communities primarily responded to changes in atmospheric carbon dioxide concentration and mean annual temperature across the last glacial-interglacial transition, rather than the moisture-balance changes before and after this transition. Therefore, the influence of this mechanism remains highly speculative.

A second explanation for the greater abundance of nEM2 during low-stand periods is that it reflects the enhanced focusing of fine-grained sediments to deep-water areas, due to resuspension and redistribution of such sediments previously deposited in shallower areas nearshore. In fact, that such sediment focusing actually occurred in Lake Chala during these particular low-stand episodes is demonstrated by the seismic-stratigraphic evidence (Moernaut et al., 2010). Moreover the fact that the relative abundance of nEM2 is lowest (repeated 0% values) between 11.0 and 9.5 ka, which marks the wettest period in the record as inferred from lake proxies and seismic data, supports our interpretation that nEM2 represents sediment re-deposition during low-stands. One might wonder why, considering the contrasting patterns of temporal variation observed in the other clastic grain-size fractions (Figs. 9 and 10), this focusing process appears to have affected only the silts of EM2. We suggest that it most probably did affect the clays of EM1, and likely also the sandy silt of EM5 to some extent, but that this influence was overprinted by one or more stronger controls on the influx of these particle populations to the lake and/or their final delivery to the mid-lake core location.

The coarse-grained EM6, which we interpret to reflect erosive input from the crater walls, is the least abundant of the four clastic grain-size fractions. Three distinct processes must be considered to explain the abundance of this sand deposited in the lake. First, sand can be flushed into the lake by strong overland flow during heavy rainfall. Indeed, highest nEM6 values (up to ~15%) occur during episodes of highest inferred precipitation (25.0–20.5 ka and 11.0–9.5 ka; Fig. 9). However, if this were the dominant mechanism mobilizing sand-sized grains towards Lake Chala, it would probably also have dominated the temporal trends in finer-grained fluvial input (i.e., nEM2), which is not the case. Second, transport of sand-sized particles from nearshore bottom areas (where the majority initially settles) to offshore areas could result from slope failure during rapid changes in lake level, both from high to low and vice versa. The occurrence of such slope failures in Lake Chala has been

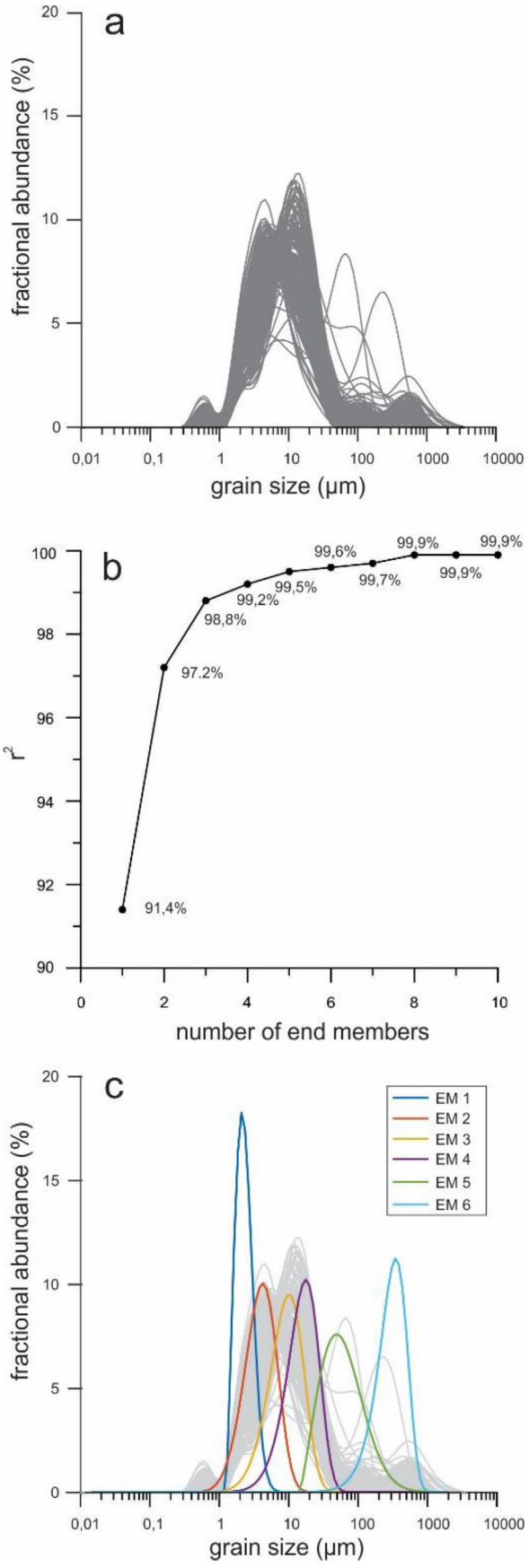

Fig. 5. End-member modeling. a) Overlay plot of the grain-size distributions (GSDs) of all samples (n = 172), illustrating the polymodal character of the Lake Chala clastic fraction. b) Increasing coefficient of determination (r^2) as a function of the number of end members (EMs) chosen to model the observed GSDs, from 1 to 10. c) The plot of all observed GSDs (grey shading) overlain with the six retained EMs (colored lines) together explaining 99.6% of the variance in the data. All EMs have a unimodal distribution, with varying width and amplitude. The GSD peak around 0.6 µm, not represented in any of the end-member model runs, is attributed to signal noise due to Rayleigh scattering upon particles >1 µm.

documented from seismic-stratigraphic evidence by Moernaut et al. (2010), who also linked several of these mass-wasting events to the turbidites that interrupt the laminated profundal sediments deposited at the core site (Fig. 6). However, this process can be excluded from discussion here because those potentially sand-rich turbidites were not analyzed in this study. The third process that can generate enhanced influx of sand-sized particles is fresh erosion of soft volcanic material near the shoreline. Local observation indicates that the highest-possible surface elevation of Lake Chala is bounded by the transition between hard volcanic rocks (locally near-vertical basalt faces) forming the lower part of the inner crater walls, and soft volcanic rocks (porous pyroclastics) forming their upper part including the crater rim (Fig. 1b). If climatic water balance were to raise the lake above this level, it would be compensated by increased outflow through the porous upper crater walls. At multiple locations around the lake, this highest-possible lake level is clearly visible as a 2–3 m high wave-cut incision forming shallow caves and overhangs at ~10–15 m above the present lakeshore. We surmise that peak values of nEM6 were realized during the times of wet climate conditions when wave action at maximum lake level eroded into porous upper crater walls and formed the above-mentioned overhangs and caves. Occurrence of this process is most obvious during the wet phase at 11.0–9.5 ka, when the abundance of nEM6 reaches its highest values (up to 43%) in the record.

Throughout the last glacial period, global dust fluxes were 10–100 times higher than during the Holocene, due to enhanced continental aridity and increased wind strength (Mahowald et al., 1999; Simonsen et al., 2019). The normalized abundance of fine distal dust (nEM1) in the Lake Chala record generally follows this pattern. Highest nEM1 abundances are found at 25-21 ka and 11-10 ka BP, with values up to 30% (Fig. 10). After 10 ka BP a rapid decline in distal dust is recorded, with generally modest amounts between 9.5 and 2.5 ka BP reaching minimum values (below 5%) at 3.5 ka BP. During the last 2.5 kyr a gradual increase in fine dust up to 15% is recorded. Temporal trends in the record of coarse dust from proximal sources (EM5) are partly opposite to those of fine distal dust (EM1), and of the temporal trends in other large-scale dust proxies (Fig. 10). Similarity with trends in nEM6 throughout the older part of the record (25 ka BP until the YD) may partly reflect incomplete separation of the two respective source populations of coarse particles by the end-member modeling, as pointed out by Dietze and Dietze (2019). Most striking is the rapid and prominent increase in nEM5 abundance to a value of ~20% shortly after the start of the Holocene (Fig. 10). High nEM5 values (10–15%) persist throughout the Holocene, increasing to an average value of 30% towards the present.

The contrasting trends of the two dust-related end members in the Lake Chala record highlight the fact that both their aeolian transport and the prevalence of their sources are controlled by different processes. Climate dynamics in equatorial East Africa are dominated by the seasonal latitudinal migration of the ITCZ and associated northeasterly and southeasterly monsoonal wind systems (Fig. 2), resulting from the interhemispheric difference in solar insolation. During episodes of expanded Northern Hemisphere glaciation, the mean latitudinal position of the ITCZ shifted southward (Broccoli et al., 2006; Mohtadi et al., 2016) and some

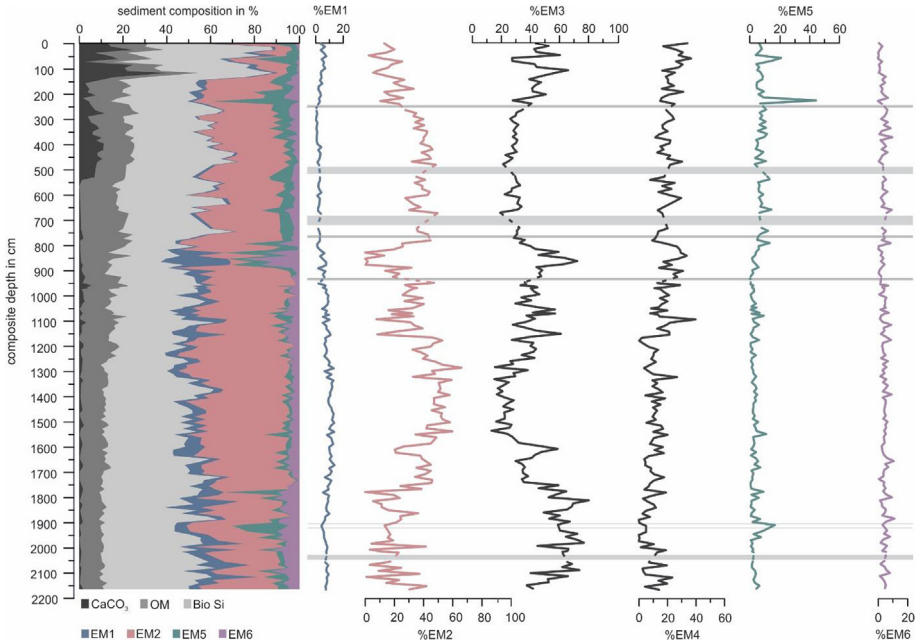

Fig. 6. Lake Chala sediment composition. Left panel: dry-mass composition (% abundance) of Lake Chala sediments with separation of calcium carbonate, organic matter and biogenic silica (grey tones), and the clastic mineral fraction as composed of the four non-diatom EMs calculated in this study (colors; see legend). Right panel: down-core variation in the % abundance of all six modeled end members (EM1 to EM6) when summed to 100% of the GSDs as measured. The grey horizontal bars show the position of event deposits (turbidites and tephra layers) not analyzed in the present study. (For interpretation of the references to color in this figure legend, the reader is referred to the Web version of this article.)

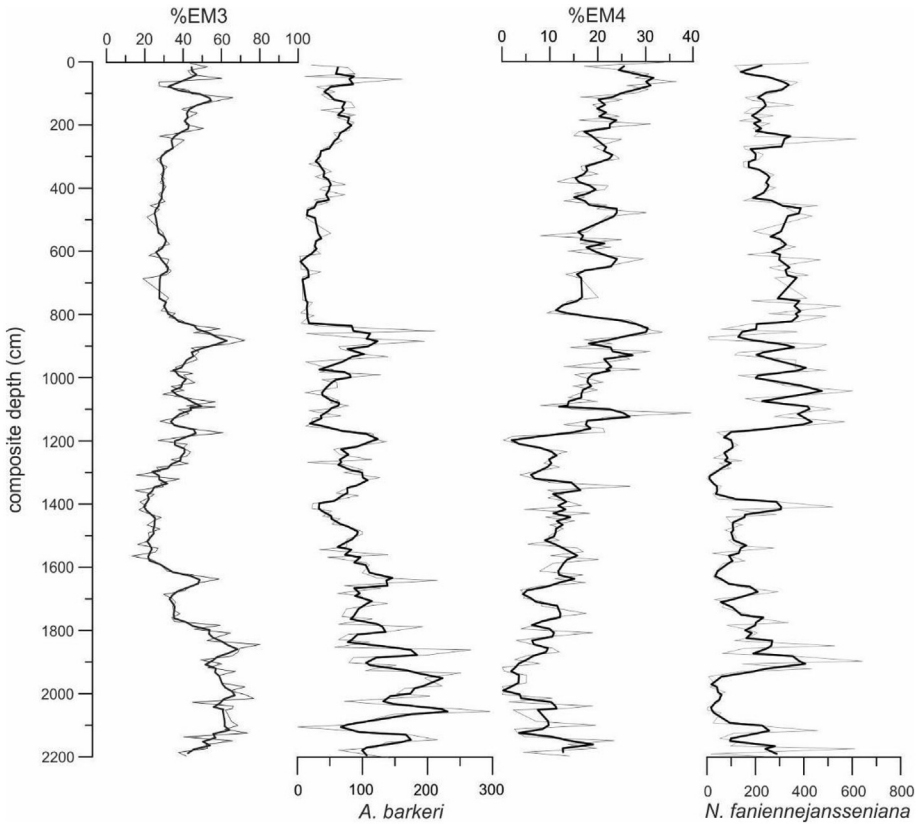

Fig. 7. Comparison between the % abundances of grain-size end members EM3 and EM4 and the absolute abundance (cell counts per mg dry mass; Milne, 2007) of the two dominant diatom species in Lake Chala sediments, both plotted against depth. Due to slight offsets between the sampling depths for both data series a 3-point running average (black lines) was calculated to permit correlation analysis.

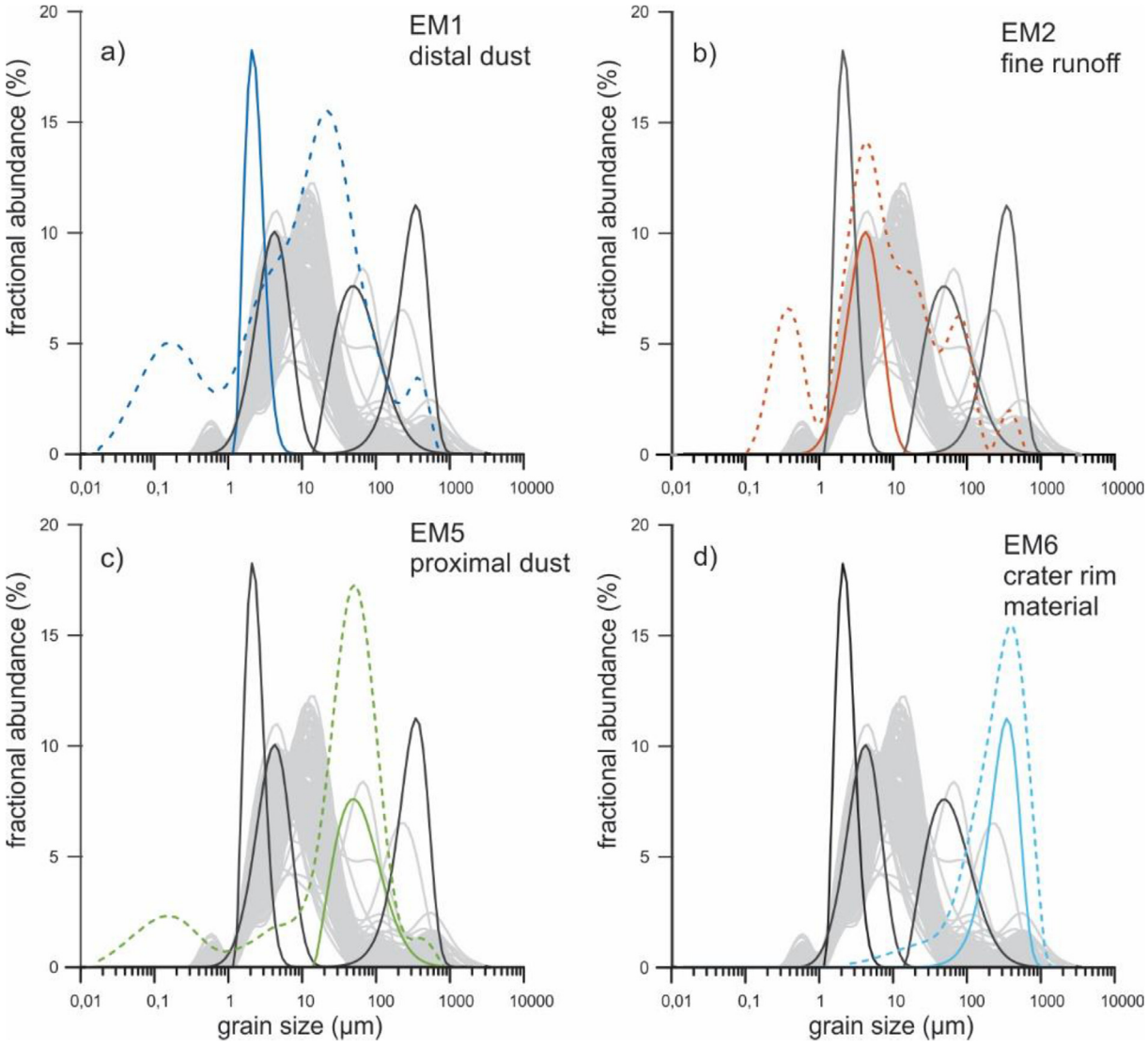

Fig. 8. Comparison of EM GSDs with the compound GSDs of four possible source materials. EM1 (a; blue solid line) is interpreted as distal dust, as it matches a clear shoulder in the combined GSD of aeolian dust collected in the Chala area during November 2016 (blue dashed line). EM5 (c; green solid line) matches the principal peak in dust collected in the town of Taveta during May 2017 (green dashed line). EM2 (b; orange solid line) is the dominant clastic-mineral component in profundal lake sediments collected in front of the creek which breaches the northwestern corner of the Chala crater rim (Fig. 1b) (orange dashed line), and is therefore interpreted to represent fine soil run-off. EM6 (d; turquoise solid line) is interpreted as coarse (sand-sized) material originating from the inner crater slopes, based on soil samples collected at the lakeshore (turquoise solid line). (For interpretation of the references to color in this figure legend, the reader is referred to the Web version of this article.)

studies indicate that this displacement of the ITCZ was also subject to other controls, such as changes in the nearby Indian Ocean monsoon system (Tierney et al., 2008; Mohtadi et al., 2014). Cooler conditions over the Eurasian continent during glacial times reduced the atmospheric pressure gradient between its southern land mass and the adjacent Indian Ocean, resulting in weaker South and East Asian monsoons (Dykoski et al., 2005). These two processes conspired to weaken southeasterly monsoon winds in equatorial East Africa, and enhance the strength (and reach) of northeasterly monsoon winds. We therefore propose that the source of the fine distal dust arriving at Lake Chala, which was on average more prominent during the pre-Holocene period, is situated in low-lying drylands of the Horn of Africa, ~1500 km northeast of Lake Chala (Fig. 2), and that this dust was transported to the Chala area by the northeasterly monsoon. This attribution is consistent with a similar glacial-to-Holocene reduction in detrital flux to the Arabian Sea (Pourmand et al., 2004), explained by these authors as caused by intensified northwesterly monsoon winds under extratropical glacial conditions, which hence advected more dust from the Arabian Peninsula. In addition, reduced evaporation from a cooler Indian Ocean sea surface during glacial episodes lowers the moisture flux onto the African continent (Tierney et al., 2008; Stager et al., 2011), generating drier conditions overall and favoring aeolian processes across the northern hemisphere tropics. Finally, lack of a comparably large source of distal dust in land areas to the southeast of Lake Chala accentuates the temporal variability in nEM1 as a northeasterly monsoon signal.

Sources of the coarse dust (EM5) in the Lake Chala record must be located closer to the lake. Land area towards the northwest is dominated by the forest-covered highlands of Mt. Kilimanjaro, lacking significant dust sources (Fig. 1a). Low-lying land areas in all other directions are covered by open savanna bush- and grassland, with patchy vegetation cover allowing soil particles to be lifted up and transported by wind (Fig. 3a). Sources of the coarser dust that is

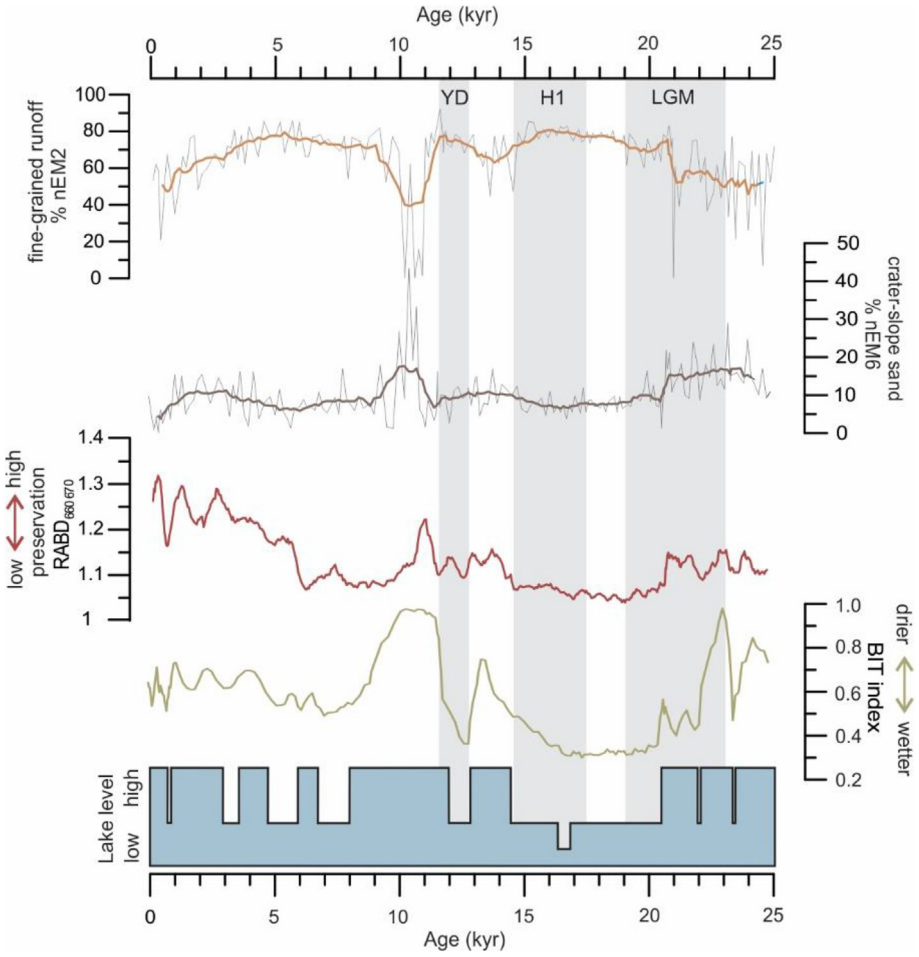

Fig. 9. Comparison between temporal variation in the normalized abundance of fine-grained runoff (nEM2) and crater-slope sand (nEM6; the thick lines are 9-point running averages) and other paleo-environmental proxies extracted from Lake Chala sediments covering the last 25,000 years: the reflectance-spectroscopic $RABD_{660\text{-}670}$ proxy reflecting algal pigment preservation (Meyer et al., 2018), the Branched and Isoprenoid Tetraether (BIT) index of regional rainfall (Verschuren et al., 2009), and the seismic-stratigraphic evidence of past lake-level fluctuation (Moernaut et al., 2010). Note that the $RABD_{660\text{-}670}$ pigment-preservation proxy is overprinted by a diagenetic gradient in the last ~6000 years, and that the seismic-stratigraphic record is semi-quantitative; the actual magnitude of lake-level change is poorly constrained. Grey bars indicate periods of glacial conditions, like the Last Glacial Maximum (LGM), and the Younger Dryas (YD) and Heinrich 1 (H1) chronozones.

mobilized by small-scale phenomena such as dust devils are certainly common in the wider landscape around Lake Chala. Considering the dominant wind directions in this area (Fig. 2c), its principal primary source may be the semi-arid savanna plains stretching up to 150 km east of Lake Chala, from where dust is advected to the lake mainly by southeasterly monsoon winds.

To explain the temporal trends in normalized abundance of EM5 over the past 25 ka (Fig. 10), a first question is to what extent changes in vegetation cover during this period may have affected the location and size of nearby dust sources. The available reconstructions of vegetation history around Lake Chala (Damsté et al., 2011; van Geel et al., 2011) indicate that during the glacial and early late-glacial periods local vegetation consisted almost exclusively of grasses, and from *ca* 14.5 ka BP onward evolved to the mixed community of grasses, shrubs and trees that was prevalent throughout the Holocene until today. Thus, contrary to what the main temporal trend in EM5 appears to indicate (Fig. 10), nearby sources of coarse dust are likely to have decreased rather than increased in areal extent across the glacial-to-interglacial transition. This apparent conflict implies that any reduction in source area relative to what it was during glacial time must have been compensated by intensification of the transport mechanism bringing the dust to Lake Chala. The deep-ocean sediment record of diatom productivity in the Arabian sea offshore Somalia (Balaji et al., 2018, Fig. 10), interpreted to reflect the upwelling intensity of nutrient-rich subsurface water masses (Jung et al., 2002), does indeed suggest that southeasterly monsoon circulation (with southwesterly winds in the Arabian Sea) was weaker during full-glacial time and again during the YD, compared with the Holocene. Lipid-based temperature reconstructions from across East Africa indicate a cooling of ~2.5 °C during the LGM compared to today at the elevation of Lake Chala (Loomis et al., 2017). A decline in land surface heating would result in a reduced occurrence of local dust events, such as dust devils, which are responsible for the transport of the coarse dust. The sharp increase in the normalized abundance of proximal dust in the Lake Chala record from *ca* 11.6 ka onwards (Fig. 10) can then be interpreted to reflect the well-documented abrupt intensification of southeasterly monsoon winds across southern tropical Africa at the YD-Holocene transition (Garcin et al., 2007; Talbot et al., 2007), and the associated resumption of 'interglacial-type' summer ITCZ migration far into the Northern Hemisphere (Verschuren et al., 2009). Interestingly, between 11.0 and 10.0 ka the abundances of both distal and proximal dust fractions are high. Our data therefore suggest that while the southeasterly monsoon responded relatively fast to global warming across the YD-Holocene transition, the northeasterly

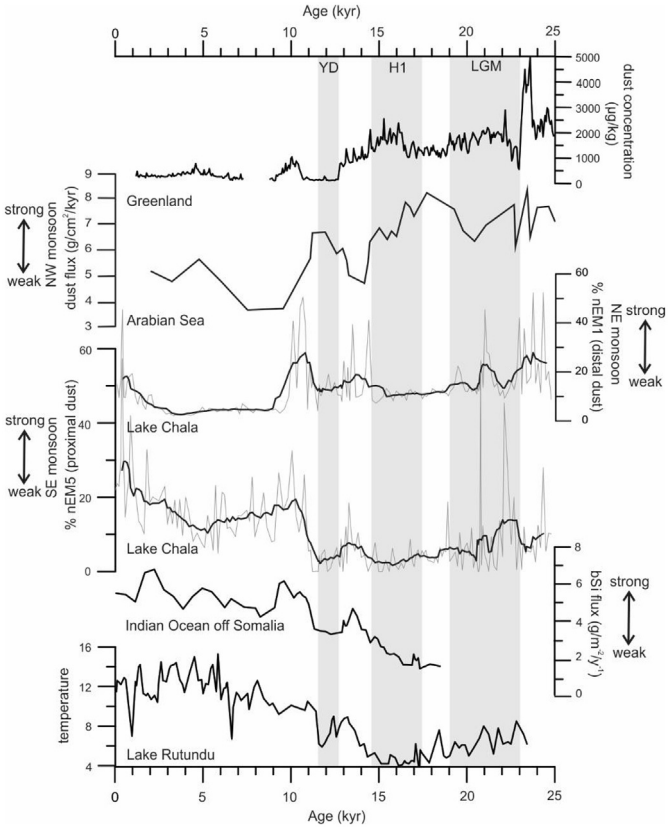

Fig. 10. Comparison of temporal variation in the normalized abundance of distal dust (nEM1) and coarser proximal dust (nEM5; the thick lines are 9-point running averages) over the last 25 kyr with selected paleoenvironmental records from elsewhere: the total dust concentration from a Greenland ice-core record (Simonsen et al., 2019) the Arabian Sea dust flux record (Pourmand et al., 2004), the bSi record of marine diatom productivity offshore Somalia reflecting the intensity of coastal upwelling (Balaji et al., 2018), and the lipid-based (brGDGT) mean annual temperature reconstruction from Lake Rutundu on Mt. Kenya (Loomis et al., 2017). The East African and Indian Ocean records are inferred to reflect climate-driven variation in the intensity of the northeasterly (NE) and southeasterly (SE) monsoons. Grey bars indicate periods of glacial conditions, namely the Last Glacial Maximum (LGM) and the Younger Dryas (YD) and Heinrich 1 (H1) chronozones.

monsoon system remained vigorous for some time, resulting in high fluxes of both distal and proximal dust. Only after the southeasterly monsoon was fully re-established, the imprint of the northeasterly source declines.

6. Conclusion

Grain-size end-member modeling of the clastic-mineral sediment fraction of the 25-kyr profundal sediment record of Lake Chala reveals valuable and independent information on climate-driven environmental changes in equatorial East Africa (and further afield) since the LGM. Observed GSDs were subdivided in statistically robust EMs, each representing a distinct particle population which could be linked to a particular type of present-day source material. By doing so, the EMs were related to different source areas and transport processes, namely fine aeolian dust from distal sources (EM1), fine catchment runoff (EM2), coarser aeolian dust from proximal sources (EM5) and coarse erosive material from the upper crater slopes (EM6). EM3 and EM4 could be attributed to the fossil frustules of two locally important diatom species, which had survived sample pre-treatment, and consequently were not considered in the paleo-environmental discussion.

Temporal variation in the relative abundance of grain-size EMs representing distal and proximal dust is shown to be a valuable indicator for past changes in monsoon circulation over equatorial East Africa. During Northern Hemisphere cold periods, such as the LGM and YD, the ITCZ and associated wind systems were pushed southward, increasing the influence of northeasterly monsoon winds in the Lake Chala area and advecting more fine dust from the Horn of Africa region. At the same time, southeasterly monsoon circulation was diminished due to a reduced pressure gradient between the East African land mass and the adjacent Indian Ocean. Despite the fact that vegetation cover was likely less complete (i.e., more patchy) during glacial time than today, mobilization of coarse dust from such proximal sources was likely more limited, due to a lesser frequency of local dust outbreaks, such as dust devils. Abrupt intensification of the southeasterly monsoon at the onset of the Holocene is recorded by an abrupt increase in the amount of coarse dust delivered to Lake Chala.

Temporal variation in the relative abundance of grain-size EMs representing catchment erosion and run-off prove to be valuable tracers of changes in sedimentation dynamics, thereby assisting the interpretation of diverse other paleoenvironmental proxies extracted from Lake Chala sediments. The *ca* 250,000-year sediment record of Lake Chala (Moernaut et al., 2010; Verschuren et al., 2013) constitutes one of the few demonstrably continuous and high-resolution natural climate archives covering such long period in equatorial East Africa, where three monsoon systems interact (Tierney et al., 2011). This study shows that subdivision of the clastic-mineral sediment fraction into statistically robust grain-size end members can provide multiple independent and quantitative proxies, which help constrain reconstructions of the region's multifaceted climate history.

Credit author statement

IM: conceptualization, methodology, investigation, writing-original draft; MVD: software, methodology, writing-review& editing; NT: investigation; MDB: Funding acquisition, writing-review & editing; DV: supervision, project administration, writing- review & editing.

Declaration of competing interest

The authors declare that they have no known competing financial interests or personal relationships that could have appeared to influence the work reported in this paper.

Acknowledgements

IM is supported by the Concerted Research Action 'Deep-CHALLA', funded by the Research Council of Ghent University. MVD is funded by the Research Foundation – Flanders (FWO). The study material was collected by the CHALLACEA project supported by FWO and funding agencies in partnering foreign institutions through the EuroCORES programme of the European Science Foundation (ESF). We thank Zainab Nduta Maina and Peter Kariuki for hosting the dust traps, and Naima Shariff for administrative help. Veerle Vandenhende and Ann-Eline Debeer are thanked for providing laboratory equipment and assistance, Christine Cocquyt for diatom SEM images, and Birgit Plessen for inorganic carbon analyses. Gert-Jan Weltje (KU Leuven) is thanked for fruitful comments on an earlier version of this manuscript, and Giovanni Zanchetta and two anonymous referees for their comments.

Appendix A. Supplementary data

Supplementary data to this article can be found online at https://doi.org/10.1016/j.quascirev.2020.106574.

References

Balaji, D., Bhushan, R., Chamyal, L.S., 2018. Variations of the Somali upwelling since 18.5 ka BP and its relationship with southwest monsoon rainfall. Clim. Past 14, 1331–1343.

Barker, P.A., Hurrell, E.R., Leng, M.J., Plessen, B., Wolff, C., Conley, D.J., Keppens, E., Milne, I., Cumming, B.F., Laird, K.R., Kendrick, C.P., Wynn, P.M., Verschuren, D., 2013. Carbon cycling within an East African lake revealed by the carbon isotope composition of diatom silica: a 25-ka record from Lake Challa, Mt. Kilimanjaro. Quat. Sci. Rev. 66, 55–63.

Barker, P.A., Hurrell, E.R., Leng, M.J., Wolff, C., Cocquyt, C., Sloane, H.J., Verschuren, D., 2011. Seasonality in equatorial climate over the past 25 k.y. revealed by oxygen isotope records from Mount Kilimanjaro. Geology 39, 1111–1114.

Ben-Israel, M., Enzel, Y., Amit, R., Erel, Y., 2017. Provenance of the various grain-size fractions in the Negev loess and potential changes in major dust sources to the eastern Mediterranean. Quat. Res. 83, 105–115.

Blaauw, M., van Geel, B., Kristen, I., Plessen, B., Lyaruu, A., Engstrom, D.R., van der Plicht, J., Verschuren, D., 2011. High-resolution 14C dating of a 25,000-year lake-sediment record from equatorial East Africa. Quat. Sci. Rev. 30, 3043–3059.

Black, E., Slingo, J., Sperber, K.R., 2003. An observational study of the relationship between excessively strong short rains in coastal East Africa and Indian ocean SST. Mon. Weather Rev. 131, 74–94.

Bodé, S., De Wispelaere, L., Hemp, A., Verschuren, D., Boeckx, P., 2020. Water-isotope ecohydrology of mount Kilimanjaro. Ecohydrology 13 (1).

Broccoli, A.J., Dahl, K.A., Stouffer, R.J., 2006. Response of the ITCZ to northern hemisphere cooling. Geophys. Res. Lett. 33.

Buckles, L.K., Weijers, J.W., Verschuren, D., Damsté, J.S.S., 2014. Sources of core and intact branched tetraether membrane lipids in the lacustrine environment: anatomy of Lake Challa and its catchment, equatorial East Africa. Geochem. Cosmochim. Acta 140, 106–126.

Cocquyt, C., Ryken, E., 2016. Afrocymbella barkeri sp. nov. (Bacillariophyta), a common phytoplankton component of Lake Challa, a deep crater lake in East Africa. Eur. J. Phycol. 51, 217–225.

Cocquyt, C., Ryken, E., 2017. Two new needle-shaped Nitzschia taxa from a deep East African crater lake. Diatom Res. 32, 465–475.

Conley, D.J., Schelske, C.L., 2001. Biogenic silica. In: Smol, J.P., Birks, H.J.B., Last, W.M., Bradley, R.S., Alverson, K. (Eds.), Tracking Environmental Change Using Lake Sediments: Terrestrial, Algal, and Siliceous Indicators. Springer Netherlands, Dordrecht, pp. 281–293.

Damsté, J.S.S., Verschuren, D., Ossebaar, J., Blokker, J., van Houten, R., van der Meer, M.T., Plessen, B., Schouten, S., 2011. A 25,000-year record of climate-induced changes in lowland vegetation of eastern equatorial Africa revealed by the stable carbon-isotopic composition of fossil plant leaf waxes. Earth Planet Sci. Lett. 302, 236–246.

Dean, W.E., 1974. Determination of carbonate and organic matter in calcareous sediments and sedimentary rocks by loss on ignition; comparison with other methods. J. Sediment. Res. 44, 242–248.

Dietze, E., Dietze, M., 2019. Grain-size distribution unmixing using the R package EMMAgeo. E&G-Quat. Sci. J. 68, 29–46.

Dietze, E., Maussion, F., Ahlborn, M., Diekmann, B., Hartmann, K., Henkel, K., Kasper, T., Lockot, G., Opitz, S., Haberzettl, T., 2014. Sediment transport processes across the Tibetan Plateau inferred from robust grain-size end members in lake sediments. Clim. Past 10, 91–106.

Dykoski, C.A., Edwards, R.L., Cheng, H., Yuan, D., Cai, Y., Zhang, M., Lin, Y., Qing, J., An, Z., Revenaugh, J., 2005. A high-resolution, absolute-dated Holocene and deglacial Asian monsoon record from Dongge Cave, China. Earth Planet Sci. Lett. 233, 71–86.

Garcin, Y., Vincens, A., Williamson, D., Buchet, G., Guiot, J., 2007. Abrupt resumption of the African monsoon at the Younger Dryas—Holocene climatic transition. Quat. Sci. Rev. 26, 690–704.

Gasse, 2000. Hydrological changes in the African tropics since the last glacial maximum. Quat. Sci. Rev. 19, 189–211.

Griepentrog, M., De Wispelaere, L., Bauters, M., Bodé, S., Hemp, A., Verschuren, D., Boeckx, P., 2019. Influence of plant growth form, habitat and season on leaf-wax n-alkane hydrogen-isotopic signatures in equatorial East Africa. Geochem. Cosmochim. Acta 263, 122–139.

Hemp, A., 2005. Climate change-driven forest fires marginalize the impact of ice cap wasting on Kilimanjaro. Global Change Biol. 11, 1013–1023.

Hemp, A., 2006. Vegetation of Kilimanjaro: hidden endemics and missing bamboo. Afr. J. Ecol. 44, 305–328.

Jung, S., Davies, G., Ganssen, G., Kroon, D., 2002. Decadal-centennial scale monsoon variations in the Arabian sea during the early Holocene. G-cubed 3, 1–10.

Just, J., Heslop, D., von Dobeneck, T., Bickert, T., Dekkers, M.J., Frederichs, T., Meyer, I., Zabel, M., 2012. Multiproxy characterization and budgeting of terrigenous end-members at the NW African continental margin. G-cubed 13, Q0AO01.

Liu, X., Vandenberghe, J., An, Z., Li, Y., Jin, Z., Dong, J., Sun, Y., 2016. Grain size of Lake Qinghai sediments: implications for riverine input and Holocene monsoon variability. Palaeogeogr. Palaeoclimatol. Palaeoecol. 449, 41–51.

Loomis, S.E., Russell, J.M., Verschuren, D., Morrill, C., De Cort, G., Sinninghe Damsté, J.S., Olago, D., Eggermont, H., Street-Perrott, F.A., Kelly, M.A., 2017. The tropical lapse rate steepened during the Last Glacial Maximum. Sci. Adv. 3.

Mahowald, N., Kohfeld, K., Hansson, M., Balkanski, Y., Harrison, S.P., Prentice, I.C., Schulz, M., Rodhe, H., 1999. Dust sources and deposition during the last glacial maximum and current climate: a comparison of model results with paleodata from ice cores and marine sediments. J. Geophys. Res.: Atmosphere 104, 15895–15916.

Meyer, I., Davies, G.R., Vogt, C., Kuhlmann, H., Stuut, J.-B.W., 2013. Changing rainfall patterns in NW Africa since the Younger Dryas. Aeolian Res. 10, 111–123.

Meyer, I., Van Daele, M., Fiers, G., Verleyen, E., De Batist, M., Verschuren, D., 2018. Sediment reflectance spectroscopy as a paleo-hydrological proxy in East Africa. Limnol Oceanogr. Methods 16, 92–105.

Milliman, J.D., Syvitski, J.P.M., 1992. Geomorphic/tectonic control of sediment discharge to the ocean: the importance of small Mountainous Rivers. J. Geol. 100, 525–544.

Milne, I., 2007. Climate and Environmental Change Inferred from Diatom Communities in Lake Challa (Kenya-Tanzania). Department of Biology, Kingston, Ontario, CanadaQueen's University.

Moernaut, J., Verschuren, D., Charlet, F., Kristen, I., Fagot, M., De Batist, M., 2010. The seismic-stratigraphic record of lake-level fluctuations in Lake Challa: hydrological stability and change in equatorial East Africa over the last 140 kyr. Earth Planet Sci. Lett. 290, 214–223.

Mohtadi, M., Prange, M., Oppo, D.W., De Pol-Holz, R., Merkel, U., Zhang, X., Steinke, S., Lückge, A., 2014. North Atlantic forcing of tropical Indian Ocean climate. Nature 509, 76.

Mohtadi, M., Prange, M., Steinke, S., 2016. Palaeoclimatic insights into forcing and response of monsoon rainfall. Nature 533, 191.

Müller, G., 1967. Methods in Sedimentary Petrology.

Nicholson, S.E., 1996. A Review of climate dynamics and climate variability in Eastern Africa. In: Johnson, T.C., Odada, E.O. (Eds.), Limnology, Climatology and Paleoclimatology of the East African Lakes. Gordon and Breach, Amsterdam, pp. 25–56.

Nicholson, S.E., 2000. The nature of rainfall variability over Africa on time scales of decades to millennia. Global Planet. Change 26, 137–158.

Paterson, G.A., Heslop, D., 2015. New methods for unmixing sediment grain size data. G-cubed 16, 4494–4506.

Pourmand, A., Marcantonio, F., Schulz, H., 2004. Variations in productivity and eolian fluxes in the northeastern Arabian Sea during the past 110 ka. Earth Planet Sci. Lett. 221, 39–54.

Prins, M.A., Bouwer, L.M., Beets, C.J., Troelstra, S.R., Weltje, G.J., Kruk, R.W., Kuijpers, A., Vroon, P.Z., 2002. Ocean circulation and iceberg discharge in the glacial North Atlantic: inferences from unmixing of sediment size distributions. Geology 30, 555–558.

Pye, K., 1987. Aeolian Dust and Dust Deposits. Academic Press, London.

Shemesh, A., Burckle, L.H., Hays, J.D., 1995. Late Pleistocene oxygen isotope records of biogenic silica from the Atlantic sector of the Southern Ocean. Paleoceanography 10, 179–196.

Simonsen, M.F., Baccolo, G., Blunier, T., Borunda, A., Delmonte, B., Frei, R., Goldstein, S., Grinsted, A., Kjær, H.A., Sowers, T., Svensson, A., Vinther, B., Vladimirova, D., Winckler, G., Winstrup, M., Vallelonga, P., 2019. East Greenland ice core dust record reveals timing of Greenland ice sheet advance and retreat. Nat. Commun. 10, 4494.

Stager, J.C., Ryves, D.B., Chase, B.M., Pausata, F.S., 2011. Catastrophic drought in the Afro-Asian monsoon region during Heinrich event 1. Science 331, 1299–1302.

Stuut, J.-B., Smalley, I., O'Hara-Dhand, K., 2009. Aeolian dust in Europe: African sources and European deposits. Quat. Int. 198, 234–245.

Stuut, J.-B.W., Prins, M.A., Schneider, R.R., Weltje, G.J., Jansen, J.H.F., Postma, G., 2002. A 300-kyr record of aridity and wind strength in southwestern Africa: inferences from grain-size distributions of sediments on Walvis Ridge, SE Atlantic. Mar. Geol. 180, 221–233.

Stuut, J.-B.W., Temmesfeld, F., De Deckker, P., 2014. A 550 ka record of aeolian activity near North West Cape, Australia: inferences from grain-size distributions and bulk chemistry of SE Indian Ocean deep-sea sediments. Quat. Sci. Rev. 83, 83–94.

Talbot, M.R., Filippi, M.L., Jensen, N.B., Tiercelin, J.J., 2007. An abrupt change in the African monsoon at the end of the Younger Dryas. G-cubed 8.

Tierney, J.E., Russell, J.E., Huang, Y., Damste, J.S.S., Hopmans, E.C., Cohen, A.S., 2008. Northern hemisphere controls on tropical southeast African climate during the past 60,000 years. Science 1160485.

Tierney, J.E., Lewis, S.C., Cook, B.I., LeGrande, A.N., Schmidt, G.A., 2011. Model, proxy and isotopic perspectives on the East African humid period. Earth Planet Sci. Lett. 307, 103–112.

Tierney, J.E., Smerdon, J.E., Anchukaitis, K.J., Seager, R., 2013. Multidecadal variability in east African hydroclimate controlled by the Indian ocean. Nature 493, 389.

Tjallingii, R., Claussen, M., Stuut, J.-B.W., Fohlmeister, J., Jahn, A., Bickert, T., Lamy, F., Rohl, U., 2008. Coherent high- and low-latitude control of the northwest African hydrological balance. Nat. Geosci. 1, 670–675.

Tsoar, H., Pye, K., 1987. Dust transport and the question of desert loess formation. Sedimentology 34, 139–153.

van Geel, B., Gelorini, V., Lyaruu, A., Aptroot, A., Rucina, S., Marchant, R., Damsté, J.S.S., Verschuren, D., 2011. Diversity and ecology of tropical African fungal spores from a 25,000-year palaeoenvironmental record in southeastern Kenya. Rev. Palaeobot. Palynol. 164, 174–190.

Verschuren, D., Olago, D.O., Rucina, S.M., Odhengo, P.O., 2013. DeepCHALLA: two glacial cycles of climate and ecosystem dynamics from equatorial East Africa. Sci. Drill. 15, 72–76.
Verschuren, D., Sinninghe Damste, J.S., Moernaut, J., Kristen, I., Blaauw, M., Fagot, M., Haug, G.H., CHALLACEA project members, 2009. Half-precessional dynamics of monsoon rainfall near the East African Equator. Nature 462, 637–641.
Weltje, G.J., 1997. End-member modelling of compositional data: numerical-statistical algorithms for solving the explicit mixing problem. J. Mathematical Geol. 29, 503–549.
Weltje, G.J., Prins, M.A., 2007. Genetically meaningful decomposition of grain-size distributions. Sediment. Geol. 202, 409–424.
Weltje, G.J., von Eynatten, H., 2004. Quantitative provenance analysis of sediments: review and outlook. Sediment. Geol. 171, 1–11.
Wolff, C., Haug, G.H., Timmermann, A., Damsté, J.S.S., Brauer, A., Sigman, D.M., Cane, M.A., Verschuren, D., 2011. Reduced interannual rainfall variability in east Africa during the last ice age. Science 333 (Suppl. l).
Wolff, C., Kristen-Jenny, I., Schettler, G., Plessen, B., Meyer, H., Dulski, P., Naumann, R., Brauer, A., Verschuren, D., Haug, G.H., 2014. Modern seasonality in Lake Challa (Kenya/Tanzania) and its sedimentary documentation in recent lake sediments. Limnol. Oceanogr. 59, 1621–1636.